The manuscript presents a valuable new micro-CT dataset from an extremely low-accumulation environment at Allan Hills Blue Ice Area (BIA), Antarctica. Such datasets are rare and of high relevance for understanding firn evolution under conditions relevant to Oldest Ice exploration. The observational work is carefully executed and the comparison with the AHMIF core (Dadic et al., 2015) is well motivated.

However, while the dataset itself is strong, the interpretation is currently not sufficiently supported by quantitative analysis, and several physical arguments are either incomplete or inconsistent. In its present form, the manuscript reads largely as a descriptive case study, while multiple causal interpretations are proposed without statistical validation.

I therefore recommend major revisions before the manuscript can be considered for publication in *The Cryosphere*.

We sincerely thank the reviewer for taking the time to give a careful and all-encompassing review. We acknowledge that the quantitative analysis in the original manuscript could be strengthened, and these comments have helped us revise, restructure, and add information to address these concerns. Broadly, the edits we performed in response to the reviewer's comments fall into the following categories for the analysis and discussion of the cores' datasets and their differences: 1) adding Wilcoxon Rank Sum tests and confidence intervals, 2) strengthening the comparison of vertical spatial variability, 3) adding age estimates for each core, 4) balancing discussion of alternative hypotheses, and 5) clarifying physical interpretations. Note that we use the abbreviations line (L) and manuscript (MS) in our responses below.

COMMENT 1. Lack of statistical testing and hypothesis validation

The manuscript proposes several hypotheses regarding the role of wind speed, surface topography, and firn exposure in controlling microstructural differences between the PICO2303 and AHMIF cores. However, no statistical tests are presented to support these claims.

- Differences in SSA, density, and structure thickness are discussed qualitatively, but it remains unclear whether these differences are statistically significant relative to within-core variability.
- At minimum, variance estimates, confidence intervals, or formal hypothesis tests comparing the two cores should be provided.
- Without such analysis, the robustness of the inferred differences remains uncertain.

We agree with the reviewer that it remained unclear whether microstructural differences are statistically significant, and that our manuscript (MS) lacked statistical tests and information. To address this comment, we perform Wilcoxon Rank Sum tests as well as calculate standard errors and provide confidence intervals on the data's best-fit lines.

Wilcoxon Rank Sum test. We calculate the Wilcoxon Rank Sum, which assesses if the pattern in the observations is from random chance and does not require a normally distributed dataset. The null hypothesis states that the median difference between observations is zero and that differences between groups is by chance. We use MATLAB's *ranksum* function and the results are listed in Table 1, where *p*-value is the probability that the null hypothesis is true; *h* is the test decision where $h=1$ indicates rejection while $h=0$ indicates failure to reject the null hypothesis at a 5% significance level; and z_s is the *z*-statistic. From Table 1, we see that the *p*-values are less than 0.05, indicating the differences between the groups are statistically significant.

Table 1. Wilcoxon Rank Sum test results for AHMIF and PICO microstructural parameters. Note that *p*-value is the probability of getting the observation result if the null hypothesis is true; *h* is the test decision where $h=1$ indicates rejection while $h=0$ indicates failure to reject the null hypothesis at a 5% significance level; and z_s is the *z*-statistic.

Parameter	ρ (z>0.6 m)	*St.Th*	*SSA* (z>0.6 m)
p value	<0.001	0.0149	0.0029
h	1	1	1
z_s	4.62	-2.43	-2.97

We add the following at L85 (Section: Introduction):: "To test if the AHMIF and PICO2303 microstructural parameters are statistically different from one another, we use the two-sided Wilcoxon rank-sum test."

We also add the following paragraph and Table 1 (L175) in Results to describe the interpretation of the Wilcoxon rank-sum test results:

"We use the Wilcoxon rank-sum test, *ranksum,* in MATLAB with an alpha value of 0.05 and sample sizes greater than 10. The layers are broken into near-surface (0 - 0.35 m) and below surface (0.6 - 5 m). However, because the near-surface data is minimal for PICO2303, we only provide test results in Table 1 for >0.6 m in order to maintain a large enough sample size for the test. We also include the value of the normal *z*-statistic, z_s, calculated from summing ranks and used to compute the *p*-value, where the sign indicates the direction of the relationship between the groups. From these test results, we observe that there are statistically significant differences ($p<0.05$) for all microstructural parameters."

Best-fit curves and confidence intervals. We previously calculated standard errors for the datasets seen in Figure 7 and 8 to calculate error bars. For additional information, we perform and add the following analysis on L175 (Section: Results):

"Additionally, we calculate the best-fit curves and r-squared values for each dataset (see Table 2) and their associated 95% confidence bands (see light shaded regions in Figure 8). Because of the high scatter in the near-surface, we take $z>0.6$ m for density and SSA for our approximations. From Table 2, we observe trends with depth and similar r-squared values for the PICO2303 and AHMIF for these intervals. The slope of St.Th(z) for PICO2303 (m=0.1400 mm m^{-1}) is slightly less than that for AHMIF (m=0.2592 mm m^{-1}) while the slope of $\rho(z)$ is greater for PICO2303 (m=19.69 kg m^{-4}) than AHMIF (m=12.40 kg m^{-4}). Additionally, the rate of decay for *SSA* for AHMIF (k=-0.2360 m^{-1}) is greater than PICO2303 (k=-0.1810 m^{-1}). Finally, the shift of curves between the two cores is most notable for $\rho(z)$ as well as *SSA(z)*."

We also add the updated Figure 8 on page 12 (Section: Results) and Table 2 on page 13 (Section: Results) in the original MS (see below).

Table 2. Best-fit curves and r-squared values for the microstructural parameters of the PICO and AHMIF cores until 5-m depth.

Parameter, PICO2303	Best-fit curve	r^2
ρ(z), kg m^{-3}	$19.69\,z + 311.5$	0.3801
St.Th(z), mm	$0.1400\,z + 0.6441$	0.9460
SSA(z), m^2 kg^{-1}	$6.154\,e^{-0.1810\,z}$	0.9195
Parameter, AHMIF	**Best-fit curve**	r^2
ρ(z), kg m^{-3}	$12.40\,z + 540.2$	0.3052
St.Th(z), mm	$0.2592\,z + 0.4175$	0.9524
SSA(z), m^2 kg^{-1}	$4.472\,e^{-0.2360\,z}$	0.9451

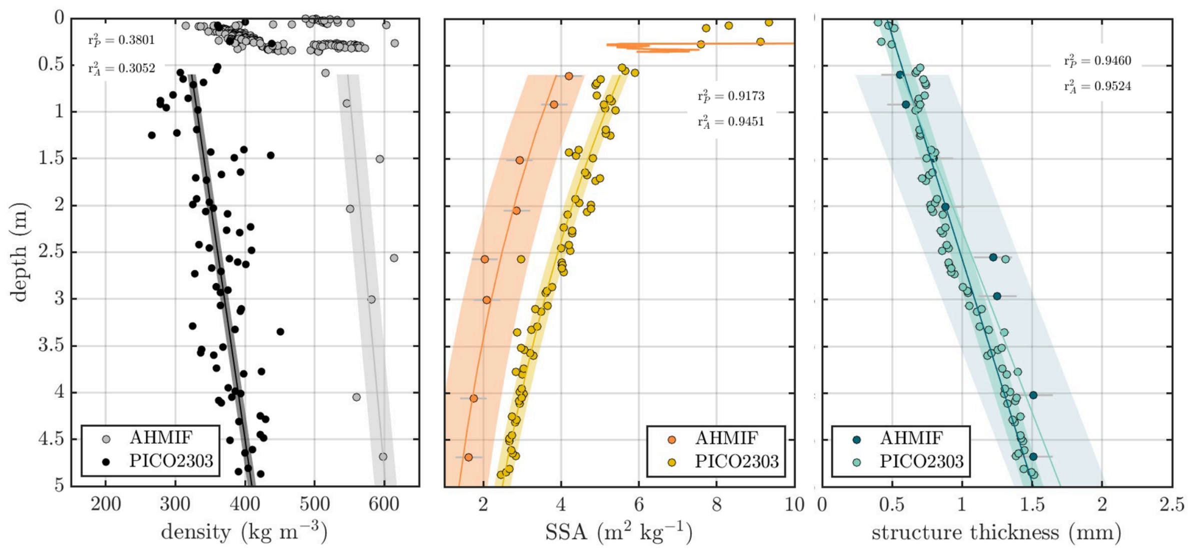

Figure 8. Comparison of parameters between the PICO2303 and AHMIF core: structure thickness (a), specific surface area (SSA) (b), and density (c). Standard errors are shown in gray bars and 95% confidence bands of best-fit lines in light-shaded regions.

COMMENT 2. Vertical spatial variability insufficiently quantified. Although vertical profiles of microstructural parameters are shown, vertical spatial variability is not explicitly analysed or discussed.

- Depth-dependent trends, regime changes, or variability within specific layers (e.g. surface layer vs. depth-hoar-dominated firn) are not quantified.
- Given the importance of vertical firn structure for permeability, ventilation, and post-depositional processes, this represents a significant shortcoming.
- The authors should consider analysing vertical gradients, depth-dependent variance, or structural breakpoints.

We appreciate the reviewer's comment and address it in three parts - depth-dependent trends, structure and layering, and gradients. We agree that more quantitative information could be provided and analyzed, and we also recognize that we had already calculated some information that the reviewer is asking for.

Depth-dependent trends. First, we have assessed depth-dependent trends and layering in multiple ways. For example, the paragraph starting on L165 of the original MS does analyze the depth-dependent trends for each microstructural parameter of the PICO2303 core (e.g., porosity, density, SSA, DA, and structure thickness):

"We use the micro-CT data to derive the parameters listed in section 2.3 (see Figure 7) to describe their variations across the full depth of PICO2303 core. Porosity decreases from 0 - 1 m (φ_{av} = 63.2%) to 11.3 m (φ = 44.8%). Density follows the inverse of porosity and increases with increasing depth to 522 kg m^{-3} at 11.3 m. Porosity and density trends correspond in part to the evolution of the depth hoar with depth (Figure 5). The observed faceted grains surrounded by large void spaces, for example, image at 0.58 m of Figure 5, are indicative of the shift to lower density and higher porosity seen above and at 0.58 m (Figure 7). Additionally, degree of anisotropy (DA) does not show a clear trend (see Figure 7), and is instead characterized by large fluctuations from around 0.15 - 0.4 (i.e. larger values mean higher degree of anisotropy) throughout the core. SSA decreases with increasing depth from 7.6 - 9.3 m^2 kg^{-1} above 0.5 m to 1.7 m^2 kg^{-1} at 11.3 m, where the rate of change of SSA decreases with depth. Finally, structure thickness increases linearly from around 0.40 mm at the surface to 2.1 mm at 11.3 m depth, where the rate of change increases at around 3.5 m."

Further, on L157, we describe the change in layers at 0.2 m from an upper fine-grained layer to a layer of large, faceted depth hoar as well as the wind crusts that are observed. We supplement this with the best-fit curve, confidence intervals, and standard errors which provides general information and is at the end of Comment 1's response and Table 2 (see above), which is added to page 12 and 13 referenced from the original MS.

Structure and layering. Second, we add more quantitative information through a description of the structure and layering as well as their associated microstructural parameter values for both PICO2303 and AHMIF in Table 3 and Table 4 below. Generally, we have described qualitatively that the AHMIF and PICO2303 cores have near-surface layers that show effects of wind processes, such as high SSA and density. However, we add the following, as well as Tables 3 and 4, into the MS starting on L175 (Section: Results). “For a more comprehensive analysis, we divide cores into layers based on changes of parameters. For example, for the PICO2303 core, there are four main layers: a near-surface fine-grained layer, two layers from the progression of depth hoar, and the coarse grains of the rest of the core (see Table 3). Further, the AHMIF core has three near-surface layers where two high-density layers sandwich one of low density (Table 4). The two coarse-grained layers at depth are divided based on the trends of the microstructural parameter changes.”

Table 3. PICO2303 layer description with mean ($\bar{x}$) and standard deviations (s) for each microstructural parameter where layers are defined as fine-grained (FG), depth hoar (DH), or coarse-grained (CG).

Depth range	Layer	ρ (kg m^{-3}) $\bar{x}$, s	St.Th (mm) $\bar{x}$, s	SSA (m^2 kg^{-1}) $\bar{x}$, s	DA $\bar{x}$, s	φ(%) $\bar{x}$, s
0.0 m - 0.30 m	FG	388.24, 32.24	0.46, 0.05	8.63, 0.75	0.37, 0.02	57.66, 3.52
0.3 m - 1.25 m	DH	312.94, 28.87	0.70, 0.02	5.25, 0.30	0.26, 0.06	65.87, 3.15
1.25 m - 3.50 m	DH	370.72, 31.03	0.92, 0.16	4.09, 0.58	0.31, 0.07	59.57, 3.38
3.5 m - 11.30 m	CG	455.74, 48.38	1.37, 0.08	2.80, 0.17	0.30, 0.06	57.41, 3.51

Table 4. AHMIF layer description with mean ($\bar{x}$) and standard deviations (s) for each microstructural parameter where layers are defined as fine-grained (FG), depth hoar (DH), or coarse-grained (CG). Note that *St.Th* is not measured above 0.6 m. See Dadic et al. (2015) for more information.

Depth range	Layer	ρ (kg m^{-3}) $\bar{x}$, s	St.Th (mm) $\bar{x}$, s	SSA (m^2 kg^{-1}) $\bar{x}$, s
0 - 0.07 m	FGwp	507.19, 24.41	-	25.51, 5.18
0.07-0.27	-	385.40, 40.49	-	11.85, 1.59
0.27-0.35	FG	500.18, 53.97	-	6.16, 0.65
0.60-2.04	CG	551.18, 32.48	0.71, 0.15	3.45, 0.66
2.04-4.68	CG	588.67, 22.77	1.37, 0.16	1.88, 0.23

Gradients. Third, we also calculate the numerical gradients of the parameters using MATLAB’s *gradient* function (see Table 5 and 6). We add the following after the layering description on L175 (Section: Results) of the original MS. “Gradients in parameters are also calculated, where these data confirm our observations (e.g., Figure 7 and 8 in MS). Within the depth hoar from 0.3 m - 1.25 m in the PICO2303 core, the gradients in density, *St.Th*, anisotropy, and porosity are opposite the neighboring layers of the PICO2303 core. This includes decreasing density and increasing porosity. Decreasing density is also observed in the AHMIF two near-surface layers (0 - 0.07 m and 0.27 m - 0.35 m) paired with increasing SSA.”

Table 5. Gradients in parameter values with depth for the core from PICO2303. We include the depth range of 3.5 m - 5 m for comparison to the depth of the AHMIF core along with 3.5 m - 11.3 m to include the entirety of the PICO2303 core.

Depth range	$\Delta\rho/\Delta z$ (kg m^{-3}m^{-1}), r^2	$\Delta St.Th/\Delta z$ (mm m^{-1}), r^2	$\Delta SSA/\Delta z$ (m^2 kg^{-1}m^{-1}), r^2	$\Delta A/\Delta z$ (m^{-1}), r^2	$\Delta\ \varphi/\Delta z$ (% m^{-1}), r^2
0 m - 0.3 m	162.26, 0.26	0.087, 0.03	-5.69, 0.53	0.07, 0.10	-17.69, 0.28
0.3 m - 1.25 m	-66.32, 0.30	-0.011, 0.012	-2.78, 0.41	-0.09, 0.11	7.23, 0.30
1.25 m - 3.5 m	5.60, 0.01	0.23, 0.73	-0.74, 0.66	0.02, 0.04	-0.61, 0.01
3.5 m - 5 m	42.12, 0.36	0.16, 0.75	-0.43, 0.69	0.03, 0.04	-4.59, 0.36
3.5 m - 11.3 m	17.47, 0.70	0.10, 0.95	-0.18, 0.90	0.01, 0.17	-1.91, 0.70

Table 6. Gradients in parameter values with depth for the core from AHMIF. Note that *St.Th* is not measured above 0.6 m.

Depth range	$\Delta\rho/\Delta z$ (kg m^{-3}m^{-1}), r^2	$St.Th/\Delta z$ (mm m^{-1}), r^2	$\Delta SSA/\Delta z$ (m^2 kg^{-1}m^{-1}), r^2
0 m - 0.07 m	-178.9, -0.03	-	194.55, 0.70
0.07 m - 0.27 m	406.86, 0.24	-	-18.92, 0.44
0.27 m - 0.35 m	-1034.0, 0.25	-	18.01, 0.60
0.60 m - 2.04 m	29.56, 0.34	0.24, 0.97	-0.99, 0.91
2.04 m - 4.68 m	-8.7, 0.14	0.16, 0.91	-0.22, 0.92

COMMENT 5. Missing age constraints on firn layers
The manuscript repeatedly refers to long exposure times (hundreds of years), yet no age estimates are provided.

- Even approximate age constraints (e.g. accumulation-based, order-of-magnitude estimates) would substantially strengthen the interpretation.
- Without age information, it is difficult to assess the persistence of microstructural features with depth or to compare the two cores in a physically meaningful way.

We agree with the feedback that approximate age constraints would substantially strengthen the interpretations within the manuscript. To address this comment, we run the Herron and Langway (1980) firn-densification model to provide estimations of age. The Herron and Langway (1980) model is a benchmark firn-densification model and is highly regarded for its simple, computationally efficient formulation. It may be limited at sites with very low accumulation rates, rapid changes in microstructure, and other non-steady state variables. However, correctly determining age through modeling efforts is prevented by the lack of data at the sites (e.g., accumulation rate at PICO2303) and is beyond the scope of this research. Thus, we use the model to provide a first-order approximation of the age of firn.

The model is in part driven by accumulation rate. From Dadic et al. (2015), the accumulation rate at AHMIF is calculated as 0.0075 m weq yr^{-1}. However, no accumulation rate estimation exists at PICO2303. In general, the accumulation rate may be highly variable in the Allan Hills BIA region and so we show age estimations using the accumulation rate calculated from a rate of 0.0075 m weq yr^{-1} at AHMIF to a rate of an order of magnitude higher, 0.075 m weq yr^{-1} (see Figure 10). To show the sensitivity of the estimations to surface density, we show estimations using both surface densities. We add the following the analysis outlined above after L175 (Section: Results):

"We estimate firn age in the upper 5 meters of the firn layer by using the Herron and Langway (1980) model. The model is considered to be a benchmark firn-densification model, as many firn-densification models developed after are based on similar assumptions (e.g., Stevens et al., 2020). To derive their densification-rate equation, Herron and Langway(1980) used depth-density data from 17 cores and Sorge's law, a steady-state assumption stating that, under constant temperature and accumulation, the relation between density and depth is invariant over time. Firn age is defined as

$$Age(\rho) = [1/(k_0 \dot{b}^a)] ln[(\rho_i - \rho_0)/(\rho_i - \rho)], \quad \rho \leq 550 \text{ kg m}^{-3}$$

and

$$Age(\rho) = [1/(k_1 \dot{b}^b)] ln[(\rho_i - \rho_{550})/(\rho_i - \rho)] + Age(550), \quad \rho > 550 \text{ kg m}^{-3},$$

where a and b are site-specific constants, $Age(550)$ is the firn age at the boundary of the second stage of densification, ρ_i is ice density, ρ_0 is surface density, ρ_{550} is the density at the boundary of the second stage, $\dot{b}$ is the accumulation rate, and k is a coefficient that incorporates an Arrhenius rate law that depends on temperature and the firn-densification zone (Herron and Langway, 1980; Lundin et al., 2017). We run the model using the accumulation rate calculated from Dadic et al. (2015), 0.0075 m weq yr^{-1}. Because the accumulation rate is unknown at PICO2303, we also run the model at 0.0135 m weq yr^{-1} intervals until an order of magnitude greater. To understand the model's age estimation sensitivity to surface density, we show these approximations using both the surface densities at AHMIF and PICO2303. "

We also add the below figure as Figure 10.

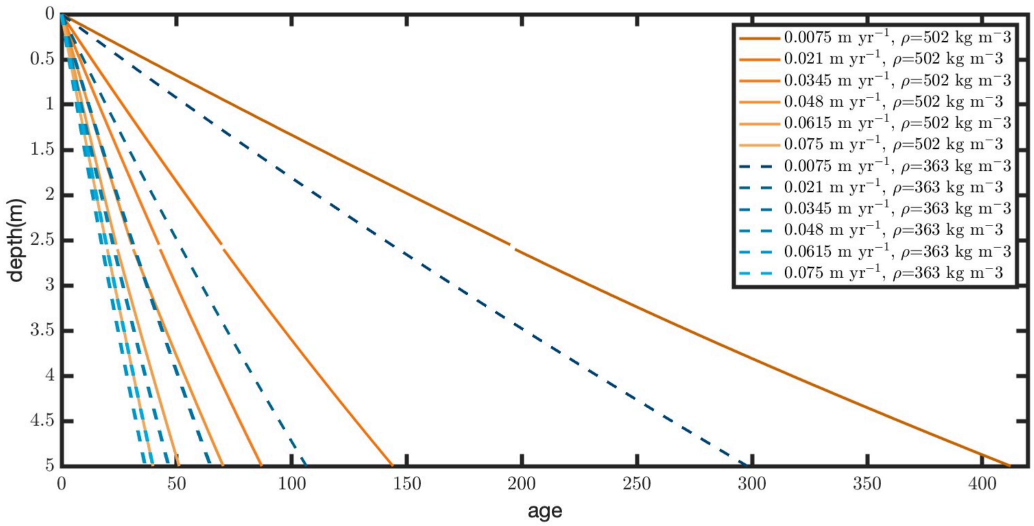

Figure 10. Age estimation of the upper 5 meters are modeled from b=0.0075 m weq yr^{-1} until 0.075 m weq yr^{-1} using surface densities at AHMIF (orange) and PICO2303 (blue) from the Herron and Langway (1980) firn-densification model.

We then include the following after L188 (Section: Discussion):

"From Figure 10, the Herron and Langway (1980) model estimates age at the bottom of the AHMIF core to be 412 years. Because the PICO2303 core is taken from a location most likely with higher accumulation, we assume that the age must be anywhere from 30 years to over 100 years. From Pb-210 data, Dadic et al. (2015) estimate that the bottom of the AHMIF core (z = 5 m) is around 660 years old using a constant accumulation rate of 0.0075 m weq yr^{-1}, which is several hundred years older than the estimate and suggests the influence of model assumptions (e.g., constant accumulation rate, no erasure of layers, etc).

We suggest that the near-surface firn of the AHMIF core must have been exposed to the surface longer than the PICO2303 core, potentially several hundreds of years. However, microstructure that is indicative of a strong, consistent TGM, such as large, faceted depth hoar, is not present. Thus, this must indicate that either 1) the accumulation rate has changed over time over the development of the AHMIF core, 2) there is the development of different microstructure (i.e. solid-type grains of a hard cohesive depth hoar) from high surface densities, and/or 3) there is an erasure of layers (e.g., wind erosion and snow redistribution) near the surface due to very low or negative accumulation. Further, Dadic et al. (2015) suggest that snow redistribution processes may be partially responsible for the Pb-210 data that suggest an abrupt age increase below 0.3 m.

They conclude that areas that experience katabatic winds, such as the AHMIF region, are acknowledged to have irregular Pb-210 profiles because of the post-depositional snow migration. Overall, the modeled estimation provides a first-order approximation but includes uncertainties, and future measurements are needed to constrain the depth-age scale at PICO2303."

COMMENT 3 (C3). Alternative hypotheses not adequately considered
The manuscript strongly emphasizes wind speed and surface topography as dominant controls, but alternative explanations are not sufficiently discussed, including:

- Differences in firn age (especially concerning the two cores) and residence time near the surface
- Temporal variability in accumulation and storm frequency
- Post-depositional vapor transport processes not directly linked to wind speed
  A more balanced discussion explicitly addressing alternative hypotheses would strengthen the scientific interpretation and avoid over-attribution.

COMMENT 6 (C6). Role of horizontal movement and advection
Horizontal ice and firn movement is mentioned but not evaluated.

- Horizontal advection may influence stratigraphy, residence time, and microstructure.
- The authors should clarify whether horizontal motion is negligible at these sites and, if not, how it may affect the comparison between PICO2303 and AHMIF.
- The velocity of the ice shield is not described.

We thank the reviewer for highlighting these concerns in Comment 3 (C3) and 6 (C6). We combine our response for these two comments. We agree that alternative hypotheses are not clearly considered, and we add these at L188 (Section: Discussion) of the MS to adequately clarify these comments. Note that the headers are provided only for clarity, and the quoted text is what we add into the MS.

"Several factors must be considered as possible contributors to the observed stratigraphy and microstructure in the PICO2303 core."

Regional velocity (C6)

Note that velocities are described in more detail under the paragraph that is added in the Introduction at L98 under the header "Velocity in the Allan Hills BIA area" in the response to Reviewer 2's comment:

"Spaulding et al. (2012) state that the estimated thinning is likely balanced by the thickening of the snow plains within the Allan Hills MIF. They suggest that estimated horizontal velocities indicate two distinct flow regimes: 1) very slow flow (<10 cm yr^{-1}), and 2) faster-moving outlet channels between MIF and the neighboring NWIF. The first is characteristic of BIAs and dictated by shallow bedrock ridges, which contribute to enhanced ablation rates causing steeper surface slopes and enhanced katabatic winds. The AHMIF core is located close to point P10, where horizontal velocities are around 0.16 m yr^{-1} (Spaulding et al., 2012). While there are no points at site PICO2303, P18 and P19 exist close by in the snow plains around 25 m lower in elevation, where GPS-based measured mean velocities of around 0.45 and 0.48 m yr^{-1}."

However, we add the discussion paragraph below at L188.

“From horizontal velocity data of Spaulding et al. (2012), Dadic et al. (2015) estimate that the bottom of the AHMIF core was 160 m upstream 1000 yrs ago, and that the core remained within the topographic depression and accumulation area it was extracted from. Similarly, if we assume the velocity at PICO2303 is around those estimated at P18 and P19, the PICO2303 core remained in the region of the snow plains during its formation.”

Variability in accumulation rate and other processes (C3)

“Despite residing in their respective regions during their formation, the cores have likely been influenced by variability in accumulation rate. Spaulding et al. (2012) state that the accumulation rate in the snow plains is highly variable because of the presence and migration of large sastrugi (up to 1 m) formed by katabatic winds. The strength and direction of the surface winds has seasonal and annual variability, which generates short-term fluctuations in the local accumulation rate. In opposition, wind erosion implies that shallow firn is exposed longer to near-surface processes. Thus, short-term fluctuations in surface winds and deposition lead to differences in the surface density layer and observed microstructure (e.g., type of depth hoar) (Pfeffer et al., 2002). For example, Dadic et al. (2015) suggest from Pb-210 activity that post-depositional migration of the snow is partly responsible for the AHMIF core’s profile where the upper 0.3 m shows distinctive layering indicative of wind erosion. This implies that any accumulation at AHMIF must have survived erosion if it was deposited at high wind speed and close to the initial density of the random close packing (Dadic et al., 2015).”

Age difference (C3)

“The long exposure times for both cores is validated by our age estimates. For the AHMIF core, our estimate using the Herron and Langway (1980) model predicts an age of 412 years at the bottom of the core (z = 5 m), which is over two hundred years younger than the age predicted by Dadic et al. (2015). Dadic et al. (2015) based their calculations on those from Crozaz and others (1964), and calculated the bottom of the core to be around 660 years old using the same accumulation rate of 0.0075 m weq yr^{-1}. For the PICO2303 core, our estimations using the Herron and Langway (1980) model range anywhere from 30 years to over 100 years at z = 5 m. This indicates a predicted age difference between the two cores of several hundred years at this depth, which may be much smaller than in reality as our modeled estimates do not include wind erosion and its potential removal of layers. Further, Dadic et al. (2015) suggest snow below 0.3 m in the AHMIF core is older than 100 years, making our age estimates underestimations even at that depth.”

Other post-depositional processes (C3)

“Other post-depositional processes may be at play as well. The density data show that 1) the mean density increase is not significant in the near surface of either core, which is likely from the lack of sufficient overburden pressure needed to instigate structural compaction; and 2) the observed decreases in density observed for both cores are likely from a decrease in mass loss from the temperature gradient. For example, upward vapor flux instigated from the temperature gradient in shallow firn may not be condensed but instead lost to the atmosphere. (e.g., Inoue et al., 2024).”

Horizontal strain

“Additionally, horizontal strain affects layer depths and metamorphism. More specifically, horizontal strain from ice-flow stresses impacts firn compaction in two ways: thinning due to dilatation and “strain softening” which arises due to the acceleration time-dependent microphysical densification processes (Horlings et al., 2021; Oraschewski et al., 2022). For example, firn-air content may be 4-6% less from horizontal strain rates of 10^{-3} per year as a result of layer thinning alone, given typical West Antarctic climate conditions (Horlings et al., 2021). On a microphysical scale, power-law creep is enhanced by horizontal stresses because it scales with the square of the effective stress and can lower viscosity, mainly impacting Stage 2 densification (Alley and Bentley, 1988). Because of the lack of sufficient overburden pressure to instigate high initial rates of creep, we assume the overall contribution of horizontal strain is negligible.”

COMMENT 4. Physical interpretation requires clarification and tightening
Several physical processes are invoked in a way that lacks clarity or precision:

- Metamorphism, compaction, and porosity reduction are sometimes conflated.
- Depth hoar formation is described as being "suppressed" under certain conditions, which is physically misleading (see specific comments).
- The links between observed microstructure, air movement, permeability, and isotope modification remain largely speculative.
  The manuscript would benefit from a clearer distinction between observations, inferred mechanisms, and speculative implications.

We change the manuscript to address this comment and provide clarity. In the Introduction, we change L24 (see Specific Comments below) to clarify the impact of metamorphism versus compaction. We also edit the parts of the MS on depth-hoar formation, including L79 and 191.

We edit and replace the MS text on air movement and isotope modification at L250 to as follows: "The Allan Hills Blue Ice Area is the source of a multitude of ancient ice cores, including the oldest ice on Earth (up to 6 million years old) (Shackleton et al., 2025). Ice that currently flows into the Allan Hills Blue Ice Area is sourced from the low-snowfall accumulation area around 20km upstream (Faure et al., 1992; Spaulding et al.). Quantifying post-depositional processes targeting where the Allan Hills ice cores originated is key to understanding alteration of the water-isotope record used for temperature reconstructions derived from these old ice cores at the Allan Hills Blue Ice Area (e.g., Hu et al., 2022).

The combination of high permeability and high winds increases water-vapor exchange between the atmosphere and the subsurface through snow and firn ventilation which promotes advection. In general, surface and subsurface processes in the snow and firn can drive kinetic fractionation. This process involves the exchange of molecules between the solid and vapor phases, modifying the stable water-isotope ratios from those originally established during snow precipitation. In just the surface snow alone, the atmospheric vapor-snow exchange may explain 36% of summertime day-to-day δ18O variability between precipitation events (Wahl et al., 2022); subsurface post-depositional impacts are less well-constrained and are therefore subject of many relatively recent studies (e.g., Town et al., 2008; Wahl et al., 2021; Wahl et al., 2022)."

Specific and technical comments

• **L 23**:
Replace *"including grain settling"* with *"structural compacton"*.

We replace this within the MS.

• **L 24**:
The statement that metamorphism generates a decrease in porosity is a problem. Metamorphism alone does not necessarily reduce porosity. Please revise and provide appropriate citations.

We thank the reviewer for catching our mistake. We eliminate the word 'metamorphism'. We add, "Structural changes are also driven by metamorphism from thermodynamic gradients without necessarily reducing porosity (e.g., Yen et al., 1981). The reference we add is: Yen, Y. C. (1981). *Review of thermal properties of snow, ice, and sea ice* (Vol. 81, No. 10). US Army, Corps of Engineers, Cold Regions Research and Engineering Laboratory.

• **L 37 ff**:
The Clausius–Clapeyron relation is invoked without explicit references. Please add relevant citations and clarify how it is applied here.

Generally, Antarctic snowfall is hypothesized to increase with temperature according to the Clausius-Clapeyron relationship, where the saturation water vapor pressure is a function of temperature (e.g., Clapeyron, 1834; Clausius, 1850; Nicola et al., 2023). Historically, temperature and accumulation rate are used as the primary drivers in many empirical firn-compaction models. In our MS, we are highlighting that sites in the Allan Hills BIA, such as AHMIF, do not follow the relationship because of other factors, such as the wind regime, which motivates studies to understand the microstructure and thus firn evolution there.

We add this at L37 (Section:Introduction): "Antarctic snowfall is hypothesized to increase with temperature according to the Clausius-Clapeyron relationship, where the saturation water vapor pressure is a function of temperature (e.g., Clapeyron, 1834; Clausius, 1850; Nicola et al., 2023). In many empirical firn-compaction models, temperature and accumulation rate are used as the primary drivers. However, regions such Allan Hills BIA with sites PICO2303 and AHMIF, do not follow the relationship because of other factors, such as the wind regime, which motivates research that aims to understand such sites' microstructure and thus firn evolution."

We add this into the MS and add the following references:

Clapeyron, É.: Mémoire sur la puissance motrice de la chaleur, Jour- nal de l'École Polytechnique, 14, 153–190, 1834.

Clausius, R.: Ueber die bewegende Kraft der Wärme und die Gesetze, welche sich daraus für die Wärmelehre selbst ableiten lassen, Ann. Phys., 155, 368–397, https://doi.org/10.1002/andp.18501550306, 1850.

Nicola, L., Notz, D., & Winkelmann, R. (2023). Revisiting temperature sensitivity: how does Antarctic precipitation change with temperature?. *The Cryosphere*, *17*(7), 2563-2583.

• **L 40 / Figure 1**:

o Is a secondary y-axis implicitly assumed?
o Please clarify the physical meaning and construction of this line.

We address this by adding the following to L37 (Section: Introduction) after the previous comment: "For Figure 1, we assume that snow accumulation changes are proportional to air temperature changes, via the Clausius-Clapeyron approximation. This approximation assumes there is a sensitivity of the saturation vapor pressure to temperature equal to 0.07 K^{-1} (e.g., Held et al., 2006). We assume that the accumulation scales with the saturation vapor pressure as a function of temperature."

• **Spatial variability of accumulation**:
Please clarify whether spatial variability in accumulation within and between the sites has been quantitatively considered.

We have elaborated on spatial variation of accumulation within the response Variability in accumulation rate and other processes (Comment 3) as well as within the response to Reviewer 2's comments.

• **L 78 / Fig 1**
Depth hoar formation is not "suppressed" at high densities; rather, a different type of depth hoar develops. Please revise and cite:

Pfeffer, W. T., and R. Mrugala (2002), *Journal of Glaciology*, 48(163), 485–494.

We thank the reviewer for this information. We revise the sentence to: "...depth hoar formation may form hard cohesive depth hoar with faceted solid-type grains joined by necks if surface densities are greater than 400 kg m^{-3}…(Pfeffer et al., 2002). We also add this reference into the MS.

• **L 92, L 95**:

Please add degree symbols (°) to longitude and latitude coordinates.

We add the degree symbols here.

Recommendation

The manuscript contains a valuable and rare dataset that is highly relevant to the Cryosphere community. However, **substantial revisions are required** to strengthen the quantative analysis, clarify the physical interpretation, and support the proposed hypotheses. I recommend **major revision**.

Martin Schneebeli

References

Clapeyron, É.: Mémoire sur la puissance motrice de la chaleur, Jour- nal de l'École Polytechnique, 14, 153–190, 1834.

Clausius, R.: Ueber die bewegende Kraft der Wärme und die Gesetze, welche sich daraus für die Wärmelehre selbst ableiten lassen, Ann. Phys., 155, 368–397, https://doi.org/10.1002/andp.18501550306, 1850.

Held, I. M., & Soden, B. J. (2006). Robust responses of the hydrological cycle to global warming. *Journal of climate*, *19*(21), 5686-5699.

Herron, M. M., & Langway Jr, C. C. (1980). Firn densification: an empirical model. *Journal of Glaciology*, *25*(93), 373-385.

Nicola, L., Notz, D., & Winkelmann, R. (2023). Revisiting temperature sensitivity: how does Antarctic precipitation change with temperature?. *The Cryosphere*, *17*(7), 2563-2583.

Pfeffer, W. T., and R. Mrugala (2002), *Journal of Glaciology*, 48(163), 485–494.

Town, M. S., Warren, S. G., Walden, V. P., & Waddington, E. D. (2008). Effect of atmospheric water vapor on modification of stable isotopes in near‐surface snow on ice sheets. *Journal of Geophysical Research: Atmospheres*, *113*(D24).

Wahl, S., Steen‐Larsen, H. C., Hughes, A. G., Dietrich, L. J., Zuhr, A., Behrens, M., ... & Hörhold, M. (2022). Atmosphere‐snow exchange explains surface snow isotope variability. *Geophysical Research Letters*, *49*(20), e2022GL099529.

Wahl, S., Steen‐Larsen, H. C., Reuder, J., & Hörhold, M. (2021). Quantifying the stable water isotopologue exchange between the snow surface and lower atmosphere by direct flux measurements. *Journal of Geophysical Research: Atmospheres*, *126*(13), e2020JD034400.

Yen, Y. C. (1981). *Review of thermal properties of snow, ice, and sea ice* (Vol. 81, No. 10). US Army, Corps of Engineers, Cold Regions Research and Engineering Laboratory.